



OPEN Effects of gradual deformation of identical and nonidentical, rotated and nonrotated U-shaped subwavelength resonators in few-layer metasurfaces

Andriy E. Serebryannikov¹, Atilla O. Cakmak²✉ & Evrim Colak³

Raising of negative-index medium has been going hand-by-hand with the exploration of quasiplanar subwavelength resonators. Now they are widely used in modern microwave, terahertz, and infrared devices, as well as in advanced physics research. Effects of stacking of the arrays of subwavelength resonators in one few-layer metasurface is connected with the key problems of modern electrical engineering, applied physics, and beyond. Recently, the interest to subwavelength resonators has been growing due to the progress in topological photonics and non-Hermitian photonics. In this paper, the selected effects of arrays coupling in a few-layer metasurface are revisited with yet uncommon focus, i.e., survival and (dis)appearance of subwavelength resonances at the gradual deformation of the resonators at a given lattice period. Microwave frequency range has been chosen to illustrate the concept. The case when the metasurfaces comprise two periodically placed U-shaped resonator arrays is considered. The sizes of the resonators are either varied simultaneously for both front-side and back-side arrays or for the back-side array only. The main purpose of this study is to explore the basic scenarios of resonance evolution in the space of geometrical parameters. It is shown that different resonances may be sensitive to the variations in geometrical parameters and to the dissimilarity between the front-side and back-side arrays to a different extent. The obtained results point to the existence of the bands, resonances, polarization-conversion and related asymmetric transmission regimes that are robust to the deformations. They can serve as the starting point in understanding the functional capability of the physical features while adjusting the size for a much wider variety of the types of subwavelength resonators. Their unveiling promises a wide avenue towards the realization of new frequency-domain and angle-domain filters, ultrathin polarization-plane convertors, asymmetric transmission devices and advanced microwave antennas.

Quasiplanar subwavelength resonators have played the key role in realization of the concept of negative-index medium^{1–3}. The progress achieved in this field enabled Transformation Optics based cloaking, chirality and polarization manipulation in quasiplanar metastructures, and advanced microwave antennas and related components^{4–10}. Understanding the effects exerted by structural deformations on transmission, reflection and polarization conversion in metasurfaces based on subwavelength resonators is important at least in two aspects: (a) in connection with the elucidation of the achievable and design of new functionalities, and (b) design of new physical scenarios that may exploit, for instance, the coupling of resonances of different types. Stacking of two or more arrays of resonators is needed for some types of polarization manipulation and filters with stop-/passbands having sharp edges. At the same time, subwavelength resonators are highly demanded in such extensively growing research fields like topological photonics and non-Hermitian photonics^{11–16}. In particular, topological modes are prospective for applications due to their robustness to the structure's deformation. Even though the resonant frequency may be shifted, such a mode survives at the deformation and remains well localized within a narrow frequency range. Generally speaking, the problem of engineering sensitivity of diverse resonances to the deformations is more general, being beyond the classical topological photonics. Moreover, engineering

¹Division of Physics of Nanostructures, ISQI, Faculty of Physics and Astronomy, Adam Mickiewicz University, 61-614 Poznan, Poland. ²College of Engineering, Grand Valley State University, Grand Rapids, MI 49504, USA. ³Department of Electrical Engineering, Ankara University, 06830 Golbasi, Turkey. ✉email: cakmaka@gvsu.edu

the desired sensitivity, e.g., weak or strong, for different subwavelength resonances in one metastructure at the same deformation should be an important step towards next-level metadevices, especially the ones capable of multifunctional operation^{17–21}.

It is worth noting that polarization manipulation is closely connected with Reciprocal Asymmetric Transmission (AT). Although a big part of the proposed AT structures exploits diffractions^{22–25}, the role of the ones using polarization manipulation is undoubtedly very important^{9,10,26–29}. Janus metasurfaces enabling asymmetric imaging and asymmetric focusing should be mentioned in the context of AT^{30–32}, which may be based on different subwavelength resonant and nonresonant elements. Besides, subwavelength resonators can be used for asymmetric excitation of (spoof) surface plasmons^{33,34}.

In this paper, we numerically study transmission, reflection, and polarization effects in the metasurfaces with the two coupled arrays of U-shaped subwavelength resonators, which are either rotated or not rotated with respect to each other. Two cases will be studied: (1) front-side and back-side resonators have the same geometrical sizes and are deformed simultaneously; (2) front-side and back-side resonators have different geometrical sizes, so the latter are only deformed. The general purpose is exploring the basic attainable features, while subwavelength resonator sizes are gradually varied. Therefore, our focus is the numerical demonstration of the achievable resonant effects, whereas their detailed theoretical analysis is beyond the scope. Consideration will be restricted to the case of linearly polarized plane waves. Most of the results will be presented in the frequency–size–scaling-coefficient plane [denoted as (f,S)-plane] in order to properly visualize effects in transmission/reflection/polarization which are yielded by the gradual variations of resonator sizes of either one of the two arrays or both arrays, in a wide frequency range. The questions to be answered include but are not restricted to the following ones: (a) when is the rotation of one of the two resonator arrays crucial (and when not) for the resonance's appearance and sensitivity, and for particular resonance scenarios, like coupling, overlapping, and merging? (b) what are the main differences between the cases when we have identical and nonidentical resonators at the front and back sides? (c) can the effects of the size scaling enable an ultimate behavior of some kind for cross-polarized transmission, including robustness to the deformations? The obtained results in the subsequent sections will primarily focus on seeking an answer to these questions.

Results and discussion

Geometry and basic relations

The unit-cell geometry of the studied bi-layer metasurfaces is presented in Fig. 1 for three values of the rotation angle between the front-side and the back-side array, $\phi = 0^\circ$, 90° , and 180° . The metasurfaces are assumed to be periodic and infinite along the x and y axes. The following geometrical parameters were chosen: $p = 15$ mm or $p = 22$ mm, $a_0 = 10$ mm, $a = Sa_0$, $w = 2.76$ mm, $g = a - 2w$, $\min(g) = 1.28$ mm, $t_{res} = 0.75$ mm and $t_{sp} = 3$ mm; S means the scaling coefficient. Two cases are considered: (i) resonators at the front side,

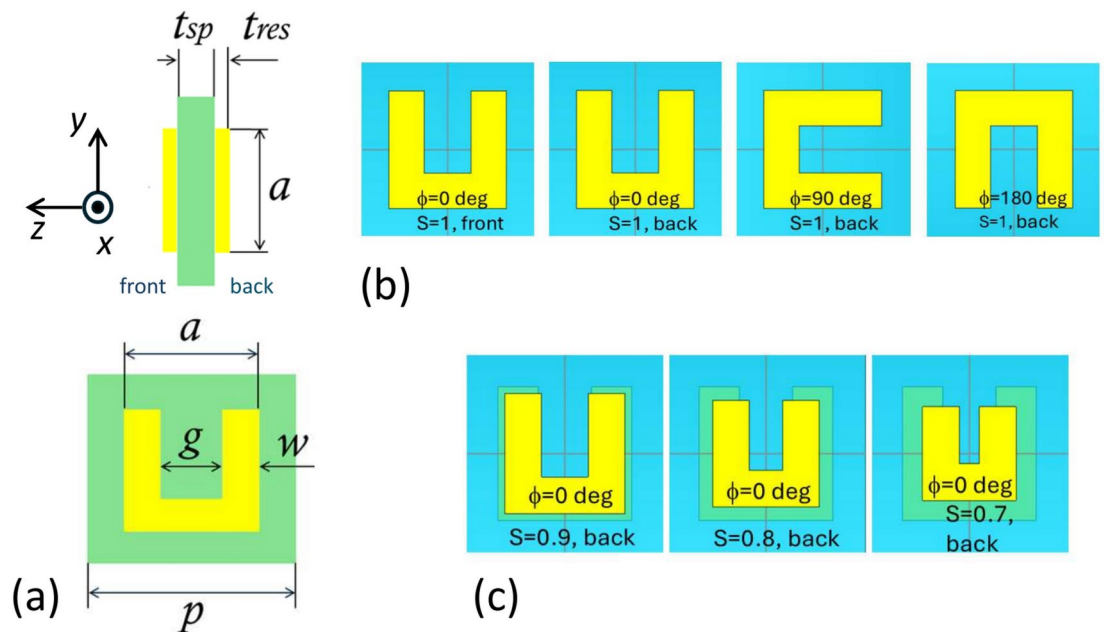


Fig. 1. Geometry of unit cells, of which the studied metasurfaces are composed: (a) explanation of the geometry of a unit cell and used coordinate system; (b) original-sized ($S = 1$) nonrotated front-side resonators and their back-side replicas at $\phi = 0^\circ$, 90° and 180° , in case of identical resonators; (c) examples of unit cells seen from the back side at different values of $S < 1$, i.e., $S = 0.9$, 0.8 and 0.7 when $\phi = 0^\circ$, in case of nonidentical resonators ($S = 1$ for the front-side resonators); when $\phi = 90^\circ$ and $\phi = 180^\circ$, the back-side resonators have the same size as shown, at the same S -values, but are rotated similarly to right and second right plots in (b).

i.e., from the side of larger z , and at the back side, i.e., from the side of smaller z , are deformed simultaneously and remain equal (S is varied), and (ii) resonators of the back side are only deformed (S is varied), while the ones at the front side are not ($S = 1$). Throughout the paper, they are referred to as the cases of *identical* and *nonidentical* resonators, respectively. Consideration is restricted to the case of normal incidence, i.e., $\theta = 0^\circ$.

In the general case, the complex amplitudes of the incident, transmitted and reflected waves are connected as follows:

$$\begin{pmatrix} T_x^\alpha \\ T_y^\alpha \end{pmatrix} = \begin{pmatrix} \tau_{xx}^\alpha & \tau_{xy}^\alpha \\ \tau_{yx}^\alpha & \tau_{yy}^\alpha \end{pmatrix} \begin{pmatrix} I_x \\ I_y \end{pmatrix}, \quad \begin{pmatrix} R_x^\alpha \\ R_y^\alpha \end{pmatrix} = \begin{pmatrix} \rho_{xx}^\alpha & \rho_{xy}^\alpha \\ \rho_{yx}^\alpha & \rho_{yy}^\alpha \end{pmatrix} \begin{pmatrix} I_x \\ I_y \end{pmatrix}. \quad (1)$$

Here, I_x and I_y are the complex amplitudes of the incident x and y polarized waves, respectively, whereas T_x^α and T_y^α indicate the complex amplitudes of the x and y polarized transmitted waves, and likewise R_x^α and R_y^α those of the reflected waves. $\tau_{xx}^\alpha, \tau_{yy}^\alpha, \rho_{xx}^\alpha, \rho_{yy}^\alpha$ stand for the co-polarized transmission and reflection coefficients, while $\tau_{xy}^\alpha, \tau_{yx}^\alpha, \rho_{xy}^\alpha, \rho_{yx}^\alpha$ do so for the cross-polarized transmission and reflection coefficients. $\alpha \rightarrow$ is used for front-side illumination and $\alpha \leftarrow$ for back-side illumination. The superscript α is omitted at $\phi = 0^\circ$ and $\phi = 180^\circ$, since $|\tau_{xx}^\alpha|, |\tau_{yy}^\alpha|, |\rho_{xx}^\alpha|, |\rho_{yy}^\alpha|$ do not depend on whether the front-side or back-side illumination is used, whereas $|\tau_{xy}^\alpha| = |\tau_{yx}^\alpha| = |\rho_{xy}^\alpha| = |\rho_{yx}^\alpha| = 0$.

At $\phi = 90^\circ$, the magnitudes of the co-polarized components are still independent on the direction of incidence, i.e., $\text{sgn}(z)$, so that α still can be omitted. However, the magnitudes of the cross-polarized components may be nonzero, depending on $\text{sgn}(z)$. Moreover, if $|\tau_{yx}^\rightarrow| \gg |\tau_{xx}^\rightarrow|$ and $|\tau_{xy}^\rightarrow| \gg |\tau_{yy}^\rightarrow|$, as may occur due to the properly designed chirality or anisotropy, then the strongly pronounced reciprocal AT may appear. This feature has been used in various AT devices^{9,10,26–29}. Clearly, the Lorentz reciprocity³⁵ states that $|\tau_{yx}^\rightarrow| = |\tau_{xy}^\leftarrow|$ and $|\tau_{xy}^\rightarrow| = |\tau_{yx}^\leftarrow|$, so that in the other possible scenario of AT we must have $|\tau_{xy}^\rightarrow| \gg |\tau_{yy}^\rightarrow|$ and $|\tau_{yx}^\rightarrow| \gg |\tau_{yx}^\leftarrow|$, assuming that the equal waves are used for the front-side and the back-side illumination, as is common for AT studies. Notably, $|\tau_{xx}^\rightarrow| \neq |\tau_{yy}^\rightarrow|$ in the studied configurations due to the structural asymmetries, regardless of the choice of ϕ . An exception may appear due to the accidental coincidence of the two coefficients. The coupling of front-side and back-side resonators, including the scenarios which lead to the well-pronounced maximums of cross-polarized transmission, can be described by the Lagrange model³⁶ or the Temporal Coupled Mode Theory^{34,37–39}, but it is beyond the scope of this study. In case when the metasurface has a perfect back-side reflector (not shown), we obtain $|\tau_{xx}^\alpha| = |\tau_{yy}^\alpha| = |\tau_{xy}^\alpha| = |\tau_{yx}^\alpha| = 0$, while the co- and cross-polarization reflection coefficients may be nonzero, also if the structure comprises only one array of subwavelength resonators. The capability of partial or full transfer of the incident-wave energy to the cross-polarized reflection has been extensively used for rotation of polarization plane for linearly polarized waves and handedness reversal for circularly polarized waves in various reflective configurations^{40–43}.

Single array of subwavelength resonators

First, let us revisit the case of single arrays of U-shaped subwavelength resonators on a finite-thickness dielectric substrate. Figure 2 presents magnitudes of reflection coefficients, $|\rho_{yy}|$ and $|\rho_{xx}|$ in (f, S) -plane for two arrays, which only differ by the lattice period, for the both x - and y -polarized incident waves. For y -polarization and $p = 15$ mm, the gaps of resonators (denoted by g in Fig. 1) are aligned with the magnetic field vector of the incident wave. Resonances of two types can be distinguished based on typical features observed in (f, S) -plane, assuming them rather than the ones of resonant near-field distribution to be a basis for classification. For the ones, which are referred to as the resonances of type A, the central frequency of the band, f_c , can be said to change weakly although the band can be quite wide and increasing while upscaling the resonators. In contrast,

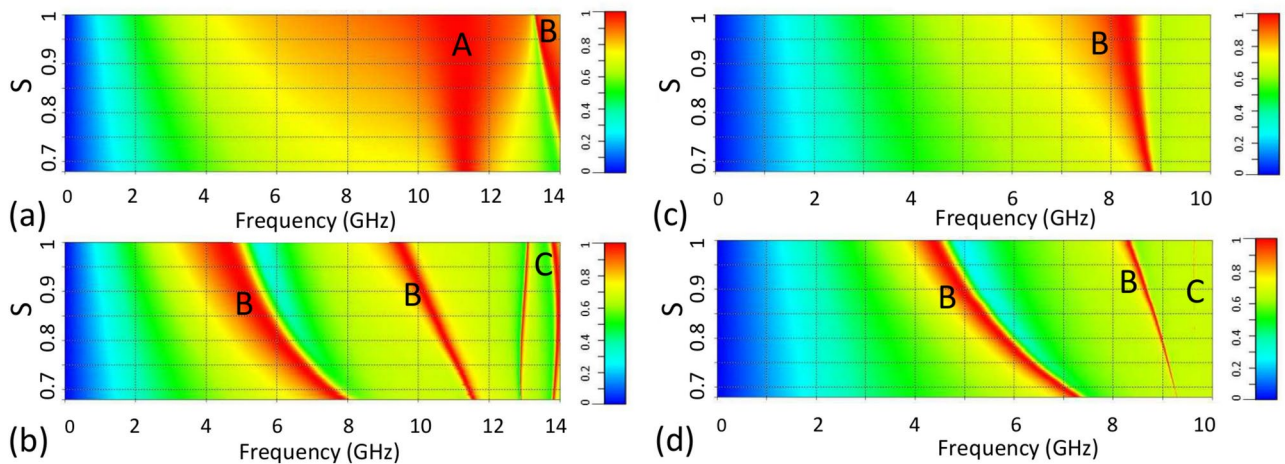


Fig. 2. Maps of (a, c) $|\rho_{yy}|$ and (b, d) $|\rho_{xx}|$ in (f, S) -plane, for a single array of U-shaped subwavelength resonators placed on the substrate being 3 mm thick, with permittivity $\epsilon_s = 5$ at $\theta = 0^\circ$. The lattice period is $p = 15$ mm (a, b) and $p = 22$ mm (c, d).

the resonances assigned to the type B are narrower and their f_c is obviously varied while scaling the resonators down. The resonances of both types are sustained within the entire range of S variation.

For the x -polarized incident waves and $p = 15$ mm, gaps of the individual resonators are aligned with the electric component field vector of the incident wave. Two resonances can be assigned as type B, whose bandwidth depends on their f_c up to a certain degree, which in turn significantly varies with S . Here, we also observe the resonances which are assigned as type C, whose typical feature is that their f_c is either nearly constant or weakly varied with S . Possible reasons of such behavior may include (a) compensation of a(n) decrease (increase) of the resonator's effective inductance by increase (decrease) of its effective capacitance while varying S , and (b) appearance of lattice resonances^{44–49}, for which the expected function of the resonators is, first of all, introduction of the required lattice period and dependence on polarization. The importance of the period choice in the appearance of resonances is clearly seen when Fig. 2a–d are compared.

Coupled arrays of subwavelength resonators at $\phi = 0^\circ$

Figure 3 presents $|\tau_{xx}|$, $|\rho_{xx}|$, $|\tau_{yy}|$ and $|\rho_{yy}|$ for the metasurface comprising two arrays of resonators separated by a dielectric spacer. In the case of identical resonators, translational symmetry is kept, but in the case of nonidentical resonators it does not. The results are presented for both x - and y -polarized incident waves, for the same array period as in the left panel in Fig. 2 ($p = 15$ mm). Forming the pass-/stopbands with the well pronounced edges and significant modification of narrowband features occur as a result of the stacking, e.g., see Refs.^{50,51}. Some features look (very) similar in the cases of identical and nonidentical resonances, but others differ significantly.

For the y -polarized waves, the wide stopband is observed between 6 and 12 GHz, whose width depends on S . It is connected with the resonance of type A. The stopband's left (lower- f) edge shows a Fano resonance shape^{13,52}. Indeed, the closely spaced regimes of (near-)zero and (near-)unity transmission are observed, for example, in the vicinity of $f = 6$ GHz at $S = 1$. They are kept for all values of S in the case of identical resonators but the observed behavior tends to significantly change in the case of nonidentical resonators when S is decreased; see Fig. 3a–d. The same Fano-type behavior remains for the right (higher- f) edge of the wide band in case of identical

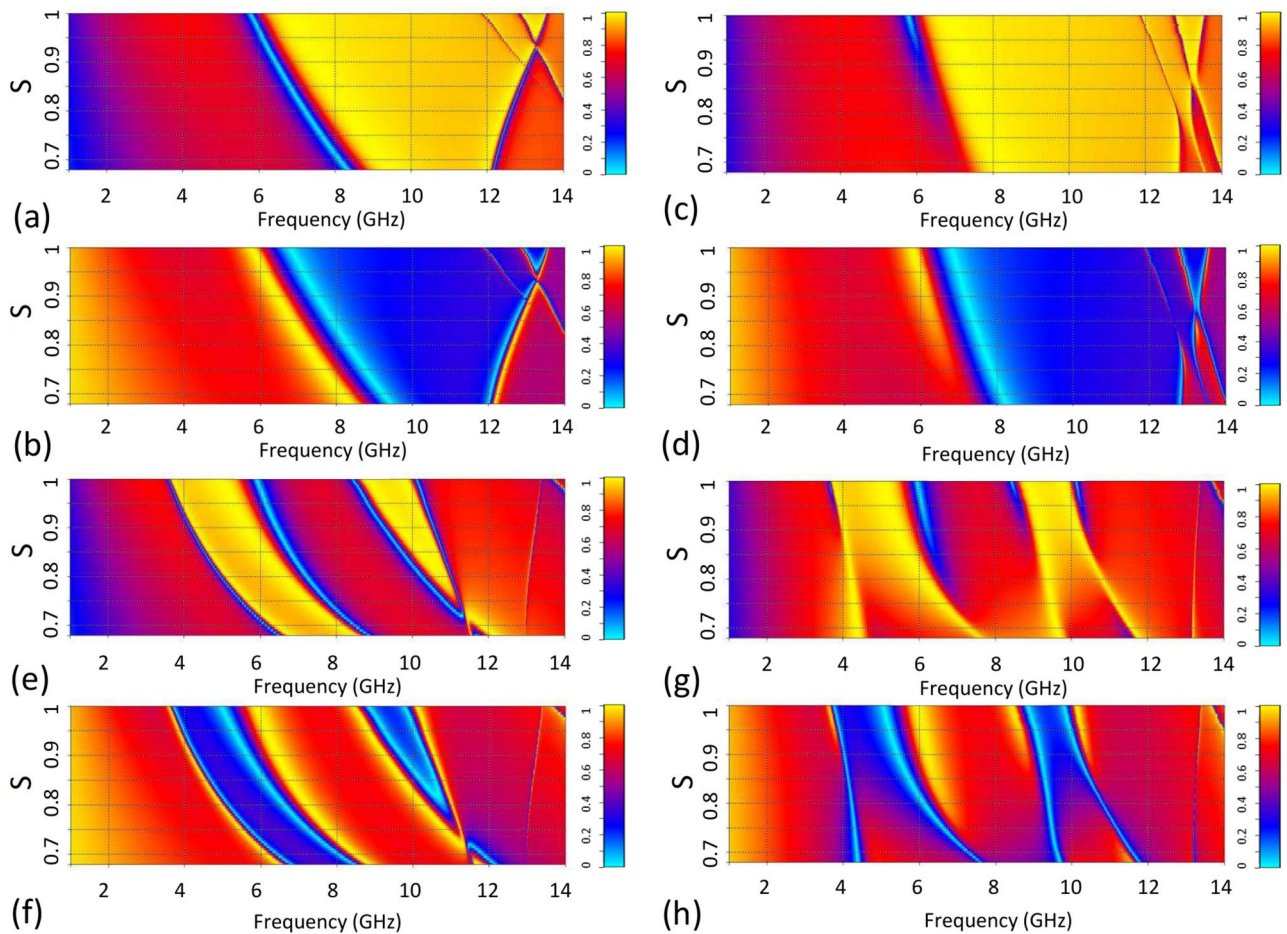


Fig. 3. Maps of (a, c) $|\rho_{yy}|$, (b, d) $|\tau_{yy}|$, (e, g) $|\rho_{xx}|$, and (f, h) $|\tau_{xx}|$ in (f, S) -plane, for a metasurface comprising two coupled arrays of U-shaped subwavelength resonators separated by the dielectric spacer with permittivity $\varepsilon_s = 5$; $\theta = 0^\circ$, $\phi = 0^\circ$, $p = 15$ mm. Left panel—case of identical resonators; right panel—case of nonidentical resonators.

resonators, at least if $S < 0.87$. In the vicinity of $f = 12.5$ GHz, we observe the overlapping of the narrowband and wideband features in transmission and reflection, so that they can suddenly be changed at a rather small variation of S , as occurs at $0.87 < S < 1$. For the given S , the observed narrowband features may remind us about defect modes^{53–55} or topological modes^{14–16}, but here it occurs in a structure with translational symmetry of the resonator arrays. A very interesting feature of the maps of $|\tau_{yy}|$ and $|\rho_{yy}|$ is that they are symmetric with respect to the vertical line around $f \approx 13.3$ GHz that may indicate the possible existence of Exceptional Point (EP)^{11–13}. For the nonidentical resonators, we obtain a more “vertical”, i.e., a less dependence on S on the left edge of the wide band in the vicinity of $f = 7$ GHz. At $f > 12$ GHz, we should notice a completely different behavior of the narrow-resonance features than in the case of identical resonators. In particular, the “mountains” of $|\tau_{yy}|$ gradually approach each other. Some of them are kept at nearly the same spectral distance from the neighbor in a wide range of S . In any case, we may obtain narrow transmission “valleys” inside the otherwise highly reflective regions in the (f, S) -plane. A partial analog of the band edges “convergence” region, which was observed in Fig. 3b near $f = 13.3$ GHz and $S = 0.93$, appears in Fig. 3d near $f = 13.25$ GHz and $S = 0.87$. However, the symmetry of the maps of $|\tau_{yy}|$ is observed for the latter only if $S > 0.87$ but it does not remain at smaller S . The map’s symmetry can be said to be protected in this case against effects of deformation at $S > 0.87$ and not protected at $S < 0.87$. One more significant difference is that we do not observe a well pronounced right (i.e., higher- f) edge of the wide band, so it is rather blurred here due to the narrowband transmission effects, some of which will be discussed in Fig. 4. The obtained results show that in case of y -polarization we need rather identical resonators for the “sharp” (nongradual) chase of wide bands by narrow resonances, like the one in Fig. 3a, b. In turn, gradual features, including the ones that may lead to resonance coupling, are typical rather for the case of nonidentical resonators.

For the x -polarized waves, two wide frequency bands are observed in the case of identical resonators almost for all S values that are connected to the resonances of type B, but the lower and the higher bands have different sensitivity to the same S variations. In particular, the aforementioned Fano resonance shapes are observed at the edges of the wide bands almost at all values of S . For the first wide band, the bandwidth is conserved within the entire range of S variation. In other words, the deformations weakly affect its width. This is the main difference between the first wide band of the y -polarized waves and those of x -polarized counterparts. The convergence of second wide band edge leads to the degeneration of this wide band near $S = 0.7$ and $f = 11.3$ GHz. Notably, the symmetry line (similar to the ones in Fig. 3b, d) can be introduced but it is not vertical now, i.e., it is deviated from $f = \text{const}$. Hence, if the appearance of an EP is expected, then it might be not a conventional case. A similar behavior has been observed on a frequency–geometric parameter plane for a single-layer metasurface comprising high-index dielectric resonators, due to the two modes with distinct symmetries that are excited in the same resonator at the same frequency^{56,57}. Yet, we showed it for the same resonators at the front and back sides in our case. In fact, they are not equal in sense of excitation conditions that can cause the observed behavior. Note that the above discussed case with an equal-frequency symmetry line (as observed for y -polarization) has

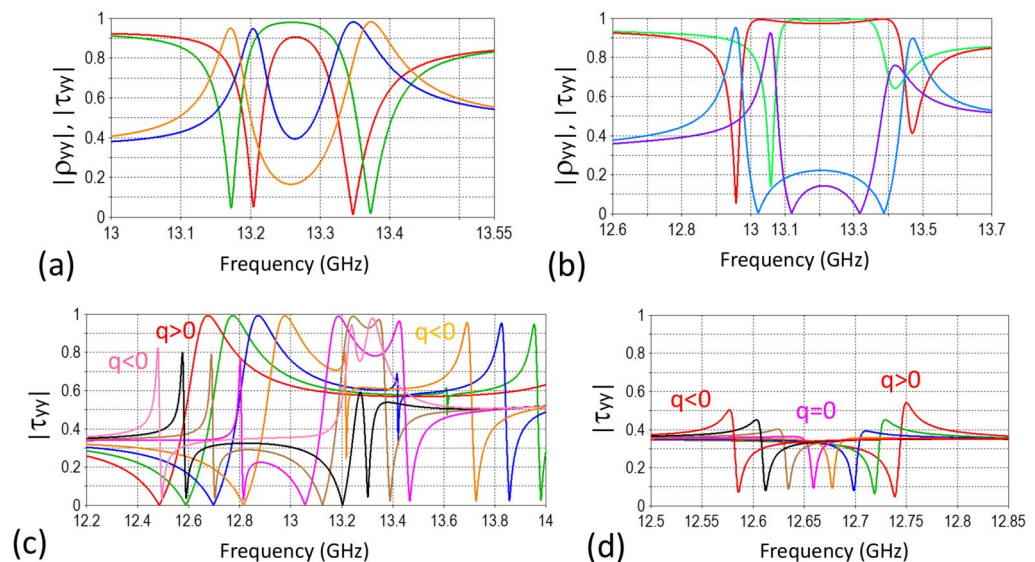


Fig. 4. One-dimensional slices of the color maps from Fig. 3: (a) $|\rho_{yy}|$ (red line) and $|\tau_{yy}|$ (blue line); and $|\rho_{yy}|$ (green line) and $|\tau_{yy}|$ (orange line) at $S = 0.95$, for the identical resonators; (b) $|\rho_{yy}|$ (red line) and $|\tau_{yy}|$ (bright-blue line) at $S = 0.91$; and $|\rho_{yy}|$ (green line) and $|\tau_{yy}|$ (violet line) at $S = 0.945$, for the nonidentical resonators; (c) $|\tau_{yy}|$ at $S = 0.81$ (red line), $S = 0.83$ (green line), $S = 0.85$ (blue line), $S = 0.87$ (orange line), $S = 0.91$ (violet line), $S = 0.92$ (brown line), $S = 0.93$ (black line), and $S = 0.94$ (rose line), for the identical resonators; (d) $|\tau_{yy}|$ at $S = 0.825$ (red line with the maximum at $f = 12.75$ GHz), $S = 0.83$ (green line), $S = 0.835$ (blue line), $S = 0.84$ (orange line), $S = 0.845$ (violet line), $S = 0.85$ (brown line), $S = 0.855$ (black line), and $S = 0.86$ (red line with the maximum at $f = 12.58$ GHz), for the nonidentical resonators.

not been achieved in Refs.^{56,57}. Besides, the narrow resonances assignable to those of type C should be noticed for x -polarization. They appear in the vicinity of $f = 13$ GHz for a wide range of S variation. In the case of nonidentical resonators, we obtain, in fact, the wide bands' gradual splitting as shown in Fig. 3g, h at $S < 0.85$. This feature can be easily explained if we take into account the fact that for two resonators with well separated resonant frequencies, the resonance appears at given f only for first of them, while the second resonator serves as a *perturbation* to the first one. The larger the difference in size between the front-side and the back-side resonators, the weaker the perturbation effect of the out-of-resonance elements is expected. This is also a reason for that some maximums and minimums are observed when S is close to 1 but disappear when S is decreased. Moreover, the lower- f band (of the two bands arising due to the splitting when S decreases), which is enabled mainly by the effects exerted by non-scaled front-side resonators with $S = \text{const}$, has a larger "slope" (i.e., it is more "vertical") than the higher- f band, which is enabled rather by back-side resonators with variable S . For instance, it can be observed in Fig. 3g, h at $4 < f < 8$ GHz. Notably, the resonance of type C, which was observed in Fig. 3e, f in the vicinity of $f = 13$ GHz, remains in Fig. 3g, h. It may indicate that the size of subwavelength resonators is less crucial in this case. For both the identical and nonidentical resonators, such a behavior of the resonances may be a signature of lattice resonances^{44–49} or guided-mode resonances^{58,59}.

Figure 4 presents several slices of the above discussed maps for the y -polarized waves, which demonstrate the features indicating possible presence of EP^{11,13} and adjustable Fano resonances^{52,60–62}. In Fig. 4a, one can see that the symmetric response, which may be associated with the vicinity of EP, can be obtained in the case of identical resonators at least at the properly adjusted structural parameters; compare to Fig. 3a–d. This result allows us to expect that EP can appear in the structures with translational symmetry, which comprise the commonly usable split-ring-type subwavelength resonators. If the resonators are nonidentical (Fig. 4b), the response is rather not associated with a vicinity of EP, because of the wide band of $|\rho_{yy}| \approx 1$ instead of a single maximum of $|\rho_{yy}|$ between two separate maximums of $|\tau_{yy}|$. Therefore, identical resonators may be needed, in order to obtain an EP for the chosen value of p and polarization state.

Next, Fig. 4c presents the examples of evolution of Fano resonance shapes at varying S , in the case of identical resonators. For the sake of better visibility of the results, we present here $|\tau_{yy}|$, but not $|\rho_{yy}|$. Rather wide passbands are formed, whose edges show Fano shapes of different polarities, i.e., different $\text{sgn}(q)$ (q is the Fano parameter)^{60–62}. It occurs at least when S is varied from 0.81 to 0.92. Moreover, narrow Fano resonances overlap with the above-mentioned wide bands, as observed at $S = 0.83, 0.85$, and 0.87 . In turn, at $S = 0.91, 0.92$, and 0.93 , the stopbands are obtained, whose edges show Fano shapes. Finally, Fig. 4d presents the examples of Fano resonances in the case of nonidentical resonators. The most interesting thing here is that polarity of Fano resonance shapes, i.e., $\text{sgn}(q)$, is changed from negative to positive when S is increased, while the case of $q = 0$ corresponding to the quasi-Lorentz shape is achieved at $S \approx 0.84$.

Coupled arrays of subwavelength resonators at $\phi = 180^\circ$

Next, we rotate the resonators of the back-side array by 180° . In such a way, we abandon translational symmetry for the both cases of identical and nonidentical resonators but still avoid cross-polarization effects. This case may also be associated with the classical double split-ring resonators, in which the gaps of the individual rings are rotated by 180° with respect to each other but in contrast to our case, they are placed on the same plane¹. Such a rotation may enable a smaller first resonant frequency at the fixed physical size, although a non-rotated performance may also have some advantages; e.g., see Ref.⁷.

Figure 5 shows the magnitudes of transmission and reflection for the metastructures comprising the same resonators as in Fig. 3, but now for the opposite orientation of the gaps at the front and the back side. For the y -polarized waves, comparison of the cases of $\phi = 0^\circ$ and $\phi = 180^\circ$ for identical resonators shows that the performed rotation does not (significantly) affect the maps of transmission and reflection, at least when $f < 10$ GHz ($\lambda/p > 2$). The same remains true for nonidentical resonators. Therefore, the presence or absence of translation symmetry is not crucial for $f < 10$ GHz. The situation becomes different when $f > 10$ GHz. Then, in the case of identical resonators, we obtain rather a gradual merging of the bands/maximums, which entirely differs from the features observed in Fig. 3a, b at $S > 0.8$. In turn, at $S < 0.8$, we do not find any significant effect of rotation of the back-side array at least for $12.8 < f < 14$ GHz. In the case of nonidentical resonators, the maps of transmission and reflection for $\phi = 0^\circ$ and $\phi = 180^\circ$ look more similar, despite some differences occurring at $f > 10$ GHz. Indeed, the narrow minimums and maximums become now even less dependent on S variations, so that they may be protected from crossings and overlaps, alternating at varying f . Note that there is no merging or coupling at the edges of the wide band near $f = 12$ GHz, in contrast with the case of $\phi = 0^\circ$; compare with Fig. 3.

The sensitivity to the 180° -rotation of the back-side array is stronger pronounced for the x -polarized waves. Then, in the case of identical resonators, we observe that (i) the first and the second wide bands are wider for $\phi = 180^\circ$ than for $\phi = 0^\circ$; (ii) there is no signature of EP for the second wide band, since it narrows not sufficiently with decrease of S ; compare to Fig. 3e, f; (iii) at $f > 11$ GHz, the maps of transmission and reflection are completely different from the ones for $\phi = 0^\circ$. In the case of nonidentical resonators, we observe in Fig. 5e, f the effects of S variation that are similar to those in the case of $\phi = 0^\circ$, at least if $f < 10$ GHz. The similarity of the cases of $\phi = 0^\circ$ and $\phi = 180^\circ$ is that the second wide band is located at $8.5 < f < 12.5$ GHz when $S = 1$, but the difference is that the edges of the single wide band remain nearly parallel at $\phi = 180^\circ$. This feature may indicate the fact that the smaller (i.e., back-side) resonators being out of resonance represent a perturbation to the larger (i.e., front-side) resonators in resonance, *to the same extent* as the larger ones being out of resonance serve as a perturbation to the smaller ones in resonance. Similarly to Fig. 3, Fano resonance shapes are typical for the edges of wide pass and stop bands, for both polarizations. The resonance regimes associated with the modes of different types are recognizable in Fig. 5.

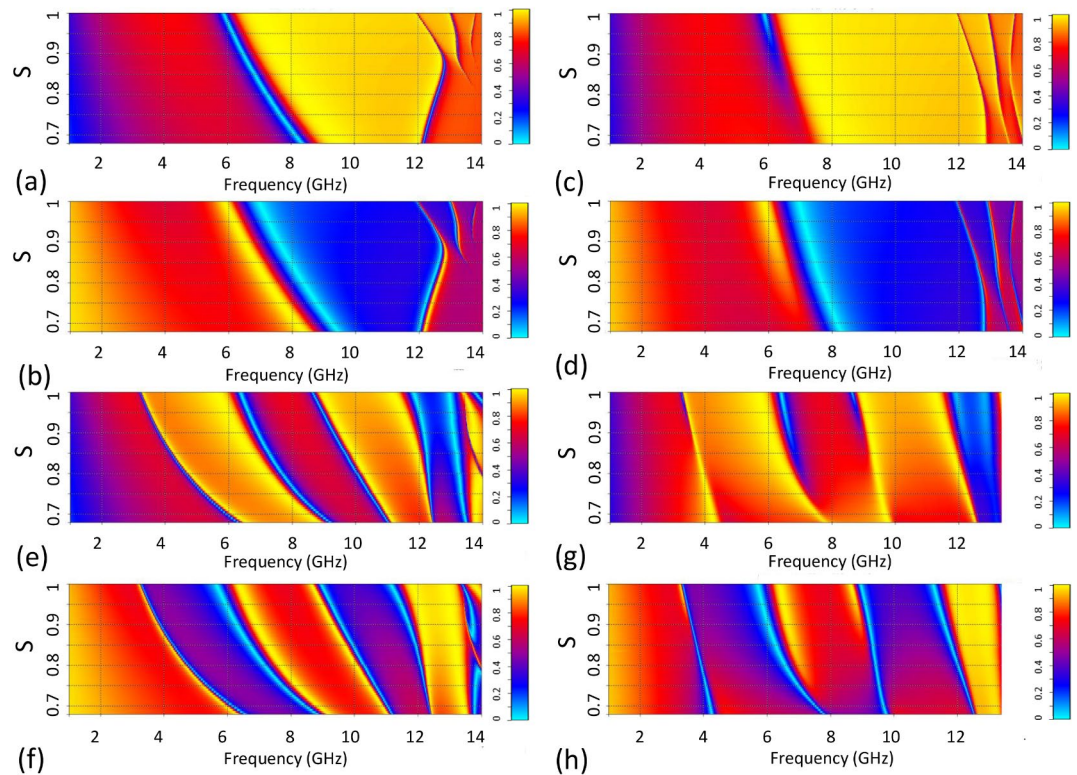


Fig. 5. Maps of (a, c) $|\rho_{yy}|$, (b, d) $|\tau_{yy}|$, (e, g) $|\rho_{xx}|$, and (f, h) $|\tau_{xx}|$ in (f, S) -plane, for a metasurface comprising two coupled arrays of U-shaped subwavelength resonators, which are separated by the dielectric spacer with permittivity $\varepsilon_s = 5$; $\theta = 0^\circ$, $\phi = 180^\circ$, $p = 15$ mm. Left panel—case of identical resonators; right panel—case of nonidentical resonators.

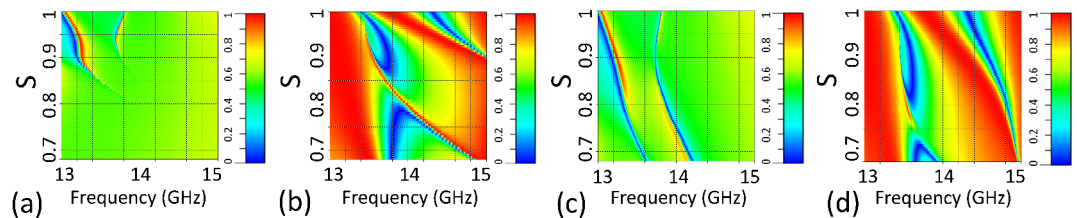


Fig. 6. Selected fragments of two-dimensional color maps of transmission partially coinciding with Fig. 5: (a, c) $|\tau_{yy}|$ and (b, d) $|\tau_{xx}|$; for (a, b) the identical and (c, d) the nonidentical resonators; the f -range extends here from 13 to 15 GHz.

Figure 6 presents $|\tau_{yy}|$ and $|\tau_{xx}|$ on the (f, S) -plane at $13 < f < 15$ GHz. In Fig. 6a, the details of overlapping Fano resonances with the moderate-magnitude wide (nonresonant) region of $|\tau_{yy}|$, and gradual disappearance of the former at decreasing S are observed. Interestingly, the sensitivity of $|\tau_{yy}|$ to the S variations for the Fano resonances (in the vicinity of $f = 13$ GHz) depends on the subrange of S , e.g. $0.9 < S < 0.95$ or $S < 0.9$. In Fig. 6b, the details of the above-mentioned narrow-“mountain”-like transmission regime are shown. Indeed, the narrow *bridge* connects two large regions of nearly-unity transmission, $|\tau_{xx}| \approx 1$, and itself preserves a nearly unitary magnitude despite of the S variations. This regime may remind us a topology-protected mode, but it is expected to be not such a classical mode, since the passbands separated by the *bridge* depend on S , and it cannot be said that we have a stopband between these passbands for all S values. Comparing Fig. 6a with Fig. 6c, we can see the differences in the appearance of Fano resonances for the cases of identical and nonidentical resonators. In particular, there is protection of some narrowband Fano-type resonant features, which remain to be overlapped with wide moderate-magnitude transmission region, in the entire range of S variation. As a result, the first and second Fano-type resonances are observed in Fig. 6c for a wider S range, which extends down from $S = 0.8$ and $S = 0.9$, respectively. Hence, $S = 1$ should be kept for resonators of at least one side, in order to prevent the possible disappearance of these resonances while decreasing S . Notably, there is the minimum frequency $f \approx 13.7$ GHz, at which the second “valley” of $|\tau_{yy}|$ is still observed; it happens when $S \approx 0.9$, and the “valley” central frequency increases at least for $S > 0.92$ and $S < 0.87$. The sign of q can be changed while varying S ,

as occurs for the second Fano resonance in Fig. 6c. The case of $q=0$ is achieved in the vicinity of $S=0.7$ for the first Fano resonance and near $S=0.9$ for the second one. Possible connection of the Fano shapes with lattice effects is noticeable. From the comparison of Fig. 6b with Fig. 6d, it is seen that the substitution of the identical resonators with the nonidentical ones results in significant changes of the map of $|\tau_{xx}|$, and, in particular, of the regions of $|\tau_{xx}| \approx 1$ and $|\tau_{xx}| \approx 0$. The features observed in Fig. 6d at $f > 13.2$ GHz are in some sense similar to those observed for the identical resonators, but a topological-like *bridge* is not observed. Some features may look similarly to this mode, but there is not a connection between the two large regions of strong transmission.

Coupled arrays of subwavelength resonators at $\phi = 90^\circ$

The metastructures comprising two identical arrays of subwavelength resonators, one of which is rotated by 90° with respect to the other, are known for the capability of rotation of the polarization plane and related asymmetry in transmission, which originate from the chirality arising at the resonances; see Refs. 6,10,26,28. Figure 7 presents the magnitudes of *co-polarized* transmission and reflection for both the *x*- and *y*-polarized incident waves at $\phi = 90^\circ$. Along with the features, which have been observed in Figs. 3 and 5, there are new ones connected with the possible partial or full conversion of the incident-wave energy to that of the cross-polarized reflection and transmission.

For the *y*-polarized incident waves and identical resonators, the consequent wide ranges of high, moderate and low transmission at $3 < f < 12$ GHz, which show the well pronounced boundaries between each other, excluding the narrow ranges of low transmission that appear at $4 < f < 8$ GHz, are easily recognizable in the reflection and transmission maps in both cases of identical and nonidentical resonators; see Fig. 7a–d. At $f > 12$ GHz, diverse features of transmission and reflection are observed, including the ones which may indicate possible merging and coupling of individual resonances. In the case of nonidentical resonators, the aforementioned transmission ranges differ, to somehow, in terms of magnitude; compare Fig. 7b with Fig. 7d. The said above remains true for reflection; compare Fig. 7a with Fig. 7e. For the nonidentical resonators, the features that weakly depend on S are kept (nearly) in the whole range of S -variation. They look very similar to the ones observed at $\phi = 180^\circ$. Also, the Fano resonance shapes at the edges of the wide bands are noticeable; e.g., see Fig. 7a around 5 GHz and Fig. 7d near 6 GHz. For the *x*-polarized waves, we also observe the wide consequent ranges of strong, moderate, and weak transmission, the boundaries between which are well recognizable. Notably, in the case of identical resonators, very similar transmission maps for *x*- and *y*-polarizations [Fig. 7(b,f)], but simultaneously

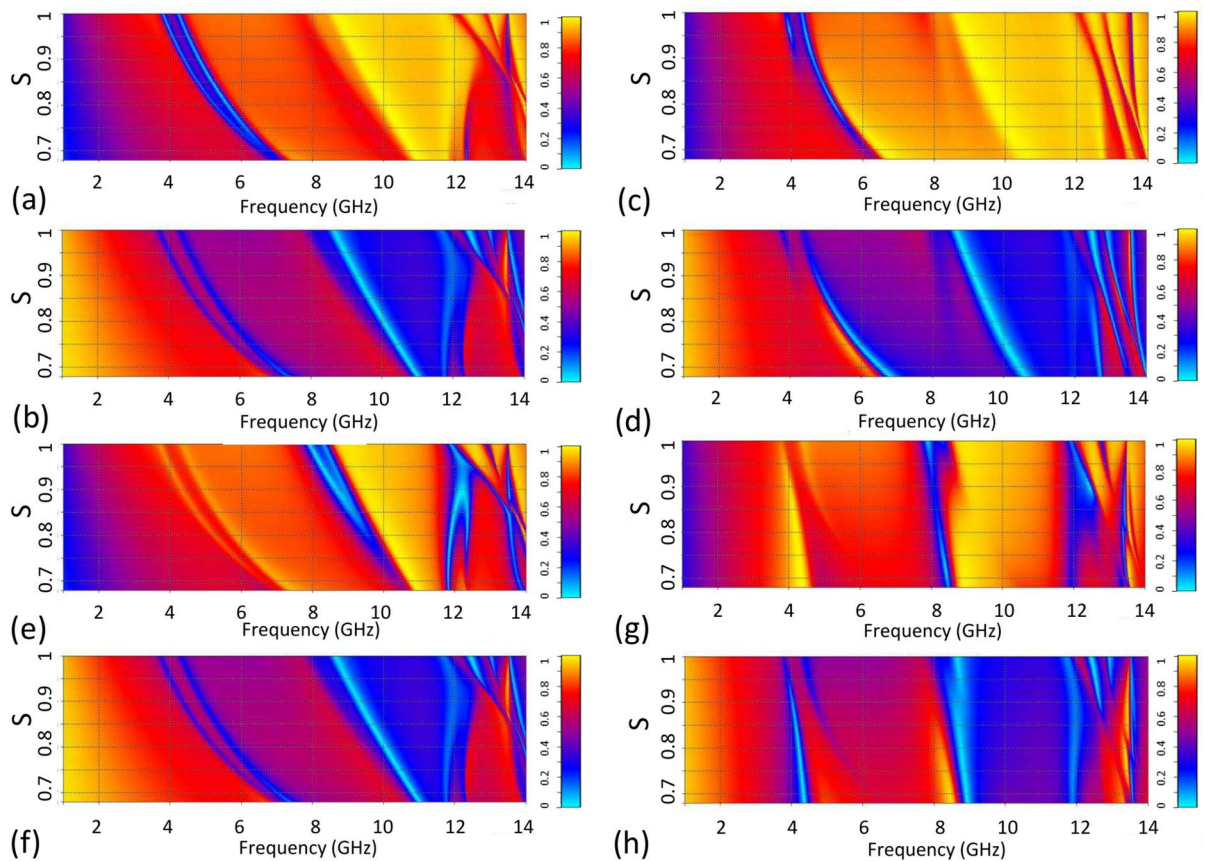


Fig. 7. Maps of (a, c) $|\rho_{yy}|$, (b, d) $|\tau_{yy}|$, (e, g) $|\rho_{xx}|$, and (f, h) $|\tau_{xx}|$ in (f,S) -plane, for a metasurface comprising two coupled arrays of U-shaped subwavelength resonators separated by the dielectric spacer with permittivity $\varepsilon_s = 5$; $\theta = 0^\circ$, $\phi = 90^\circ$, $p = 15$ mm. Left panel—case of identical resonators; right panel—case of nonidentical resonators.

quite different reflection maps (Fig. 7a, e) are observed. For the case of nonidentical resonators, the effect of polarization is rather strong for both transmission (Fig. 7d, h) and reflection (Fig. 7c, g). Fano resonance shapes similar to the ones occurring in transmission at $S < 0.85$ in the vicinity of $f = 5.5$ GHz for the y -polarized waves in the case of nonidentical resonators, appear for the x -polarized waves near $f \approx 8$ GHz; compare Fig. 7d with Fig. 7h. At the same time, the range of $|\rho_{xx}| \approx 1$ appears at 4 GHz in Fig. 7g, but it does not have analog in Fig. 7e, so that nonidentical resonators are required to obtain it. Although substitution of the identical resonators with the nonidentical ones typically leads to the appearance or enhancement of the “vertical” features on the (f, S) -plane (i.e., of narrow minimums and maximums of reflection and transmission, which do not depend or weakly depend on S), they may also occur in the case of identical resonators. One more interesting regime is observed for the nonidentical-resonators case at 11.9 GHz in Fig. 7g when both transmission and reflection are weak for all values of S . As it will be clarified below, this behavior is related to the dominant contribution of the cross-polarized components; also see Fig. 8. Similarly to y -polarization, the range of $f > 12$ GHz is characterized by a variety of narrowband resonant features that show different sensitivity to the same variations in S . Notably, Fano resonance shapes may appear in the narrow-feature ranges, i.e., at $f > 12$ GHz, for both identical and nonidentical resonators.

Next, we explore *cross-polarized* effects arising in the same metastructure. We restrict here our consideration to transmission, since it is connected with the most interesting polarization-manipulation enabled physical scenarios like reciprocal AT. Figure 8 presents the maps of $|\tau_{xy}^{\rightarrow}|$ and $|\tau_{yx}^{\rightarrow}|$ in the (f, S) -plane. Let us first consider the case of identical resonators. For the y -polarized incident waves, two closely spaced maximums of $|\tau_{xy}^{\rightarrow}|$ are kept within almost the whole range of S variation, at least when $3.5 < f < 7.5$ GHz. Only if S is small enough, e.g., $S \approx 0.7$, these maximums tend to merge, as observed in Fig. 8a. Unexpectedly, a moderately high $|\tau_{xy}^{\rightarrow}|$ occurs at $f = 12.3$ GHz but only at $S < 0.75$, so that a particular combination of a lattice period and a resonator size (a/p) is important. The detailed analysis of the optimal choice of a/p is beyond the scope. For the x -polarized incident waves, the lowest- f range of the cross-polarized transmission is observed at $7.5 < f < 10.5$ GHz, i.e., at higher f than for y -polarization; compare Fig. 8b with Fig. 8a. This feature is quite common for the coupled arrays of subwavelength resonators, being pre-determined by the properties of the individual resonators. Compared to the case of y -polarized incident waves, it looks rather like a single wide band, i.e., it does not show two separate maximums. However, the most interesting feature is observed in Fig. 8b in the vicinity of $f = 12$ GHz, where a nearly total conversion of the incident-wave energy to that of the cross-polarized transmitted wave is achieved in the *entire* range of S variation, although the bandwidth and spectral location of the band vary with S . Based on the obtained results, we can confirm the robustness of the resonances responsible for strong cross-polarized transmission results and, in turn, for the robustness of AT to the applied size changes. At $f > 12$ GHz and $S > 0.93$, and at $f > 13$ GHz ($\lambda/p < 1.53$) and $S < 0.93$, we observe in Fig. 8b a complicated pattern yielded, in particular, by merging/coupling of diverse resonances, which invokes a detailed study. Nevertheless, these regimes are not expected to be most prospective candidates from the point of view of polarization-plane rotation.

In the case of nonidentical resonators, i.e., when we only vary the sizes of back-side array’s resonators, the lowest- f band of $|\tau_{xy}^{\rightarrow}|$ observed in Fig. 8c disappears when S is still far from S_{min} . We can see that the two close but separated resonances, which are observed at $3.8 < f < 5$ GHz, show *different sensitivity* to the S variation. In particular, $|\tau_{xy}^{\rightarrow}| < 0.2$ when $S < 0.785$ for the first resonance of the pair, but $|\tau_{xy}^{\rightarrow}| < 0.2$ when $S < 0.705$ for the second resonance of this pair. Moreover, the “tail” of the second resonance is continued down to $S_{min} = 0.68$. The analog of the lower- S band of moderate $|\tau_{xy}^{\rightarrow}|$ that is observed in Fig. 8a at $f = 12.3$ GHz does not appear in Fig. 8c, so the equality of the back- and front-side resonators is necessary in this case. The behavior observed in Fig. 8c at $f > 12.3$ GHz is similar to the case of the identical resonators. However, it differs by showing the signatures of diverse resonant regimes. For the x -polarized incident waves, the lowest- f high-transmission band is also kept in the vicinity of $f = 8$ GHz, while only varying the sizes of back-side resonators,

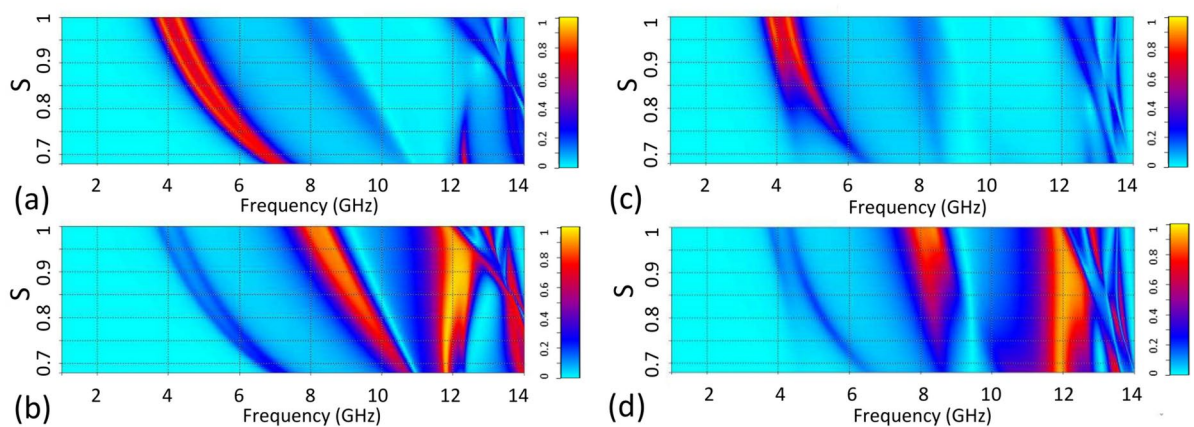


Fig. 8. Maps of (a, c) $|\tau_{xy}^{\rightarrow}|$ and (b, d) $|\tau_{yx}^{\rightarrow}|$ shown in (f, S) -plane, for a metasurface comprising two coupled arrays of U-shaped subwavelength resonators separated by the dielectric spacer with permittivity $\epsilon_s = 5$; $\theta = 0^\circ$, $\phi = 90^\circ$, $p = 15$ mm. Left panel—case of identical resonators; right panel—case of nonidentical resonators.

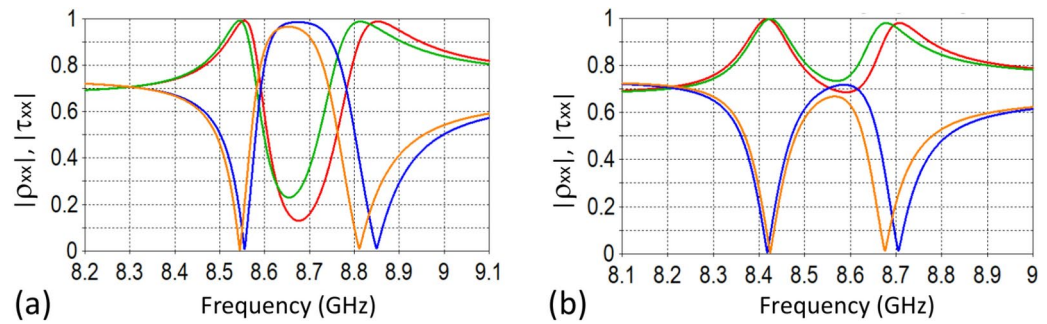


Fig. 9. (a) $|\rho_{xx}|$ and $|\tau_{xx}|$ at $S = 0.945$ (red line for reflection and blue line for transmission) and $S = 0.95$ (green line for reflection and orange line for transmission) for the identical resonators; (b) same as (a) but for the nonidentical resonators; $\theta = 0^\circ$ and $\phi = 0^\circ$, $p = 22$ mm.

but it disappears still at rather large S ; see Fig. 8d. Also in this case we may expect different sensitivities from the two closely spaced resonances in the pair, which tend to form the band, to the same variation in S . In turn, the all- S cross-polarized transmission band observed in Fig. 8b at $f = 12$ GHz also appears in the case shown in Fig. 8d; it is affected by neither the fact that the resonators are nonidentical nor the fact that S is varied in a wide range. Its similarity to the resonant band observed at $f = 12$ GHz in Fig. 8b may occur due to a lattice resonance, or the joint effect of a lattice resonance and a higher-order resonance of U-shaped resonators. Notably, this resonance is expected to be different, at least in terms of bandwidth, from the recently studied lattice resonances^{44–48}, as well as from the resonances assigned above to the type C, like the ones in Fig. 3e–h, which may have the lattice nature. But what is most interesting is that it occurs in the case when the incident-wave energy is almost entirely transferred to the cross-polarized transmission component, which is typical for the metastructures with the rotated back-side array due to the chirality arising at resonances. The lower- f edge of the discussed band that is located at $f = 12$ GHz and shows weak sensitivity to S -variations. It becomes even more vertical in the (f, S) -plane, i.e., now it is even less sensitive to the variations in S than in the case of identical resonators. Therefore, AT is robust in this case not only in sense of the conservation within the entire S -range, but also from the standpoint of the conservation of the operating frequency under physical deformations. It is worth to remind about a similar (but not so well pronounced) effect, when high capability in cross-polarized transmission and AT are conserved within the entire range of polarization angle variation, while the sizes of the few-layer metasurface comprising U-shaped resonators are kept fixed⁶³. Finally, it is noteworthy that the behavior of $|\tau_{yx}^{\rightarrow}|$ at $f > 12.7$ GHz in Fig. 8d is similar to that in Fig. 8b, so it is characterized by merging and overlapping the resonances which may have different properties. It is interesting that the topological-like *bridge* occurs in $|\tau_{yx}^{\rightarrow}|$ at $f = 13$ GHz and $0.85 < S < 0.93$, as observed in Fig. 8b. It is achieved only in the case of identical resonators. In contrast with the case of $\phi = 180^\circ$, it is achieved now in the cross-polarized transmission.

Coupled arrays at larger lattice period

In this section, we briefly discuss the selected features found for a larger lattice period. Figure 9 presents the examples of the nearly symmetric response of $|\rho_{xx}|$ and $|\tau_{xx}|$, which are achieved at $S \approx 0.95$, i.e., at the same values of S as in Fig. 4a. But now, in contrast with the case of $p = 15$ mm, we observe the symmetry of the response for the both identical and nonidentical resonators and, moreover, for the orthogonal polarization state. It is worth noting that in contrast with Fig. 4, the mid-maximum observed here near 8.6 GHz belongs to transmission. Hence, the value of p should be carefully chosen if appearance of EP is aimed for given sizes of subwavelength resonators and polarization of the incident wave.

At least two more features, which are not observed at $p = 15$ mm, should be mentioned (not shown). The first of them is the S -independent right (higher- f) edge of the wide band of large $|\tau_{xx}|$. This feature is similar in the cases of single and double resonator array. This edge can be said to be protected against the applied deformations. The second feature is that the all- S wide range of $|\tau_{yx}^{\rightarrow}| \approx 1$ at $\phi = 90^\circ$ is absent. Instead, we observe a similar band, but only at rather large values of S . Therefore, the choice of p is crucial also for protection of this cross-polarization effect against the variations in S . It is worth noting that the field distributions look similar in this case at $p = 22$ mm (when it is not an all- S effect) and at $p = 15$ mm (when it is an all- S effect), provided that $|\tau_{yx}^{\rightarrow}|$ is rather large. The obtained results allow us expecting that this effect appears owing to the mode of the same origin, i.e., it may be expected to belong to the class of lattice resonance modes.

Concluding remarks

To summarize, we revisited the selected transmission, reflection and polarization effects in the metasurfaces comprising arrays of identical and nonidentical U-shaped quasiplanar metallic resonators, while gradually deforming resonators of one or both arrays. The obtained results show that there are resonant effects in reflection and transmission, which are weakly sensitive, and the ones which are strongly sensitive to the deformations of either both the front-side and the back-side resonators or only back-side resonators, for the given angle of rotation of the arrays with respect to each other (ϕ) and the selected polarization state of the incident wave. Moreover, there are such features that are significantly sensitive to whether $\phi = 0^\circ$ or $\phi = 180^\circ$ is used, as well

as the features being weakly sensitive to the 180° rotation. According to the obtained results, such features can be observed for both cases of the identical and nonidentical resonators located at the front and the back side of the metasurface. At the 90° angle between the arrays, which is commonly associated with the capability of chirality and related asymmetric transmission (AT), the 90° rotation of the polarization plane, which is needed for well-pronounced AT, can be achieved for the x -polarized incident waves in the *entire* range of variation of the size scaling coefficient (S), at the given frequency. This resonant regime is expected to be an advancement as compared to the earlier studied narrowband resonances, like lattice and guided-mode resonances. In turn, for the y -polarized waves, it is necessary that the front-side and the back-side resonators have (nearly) the same size to conserve this AT regime for the whole range of the S variation. Moreover, at $p < \lambda < 1.75p$ (p is array period, λ is free-space wavelength), there is a variety of the effects that manifest “mountain”-like and “valley”-like features in the (f, S) -plane (f is frequency).

Most of the aforementioned transmission and reflection features observed in (f, S) -plane are worth to be carefully revisited, one by one, in order to establish an unambiguous connection between them and underlying physics. It will be a subject of our future studies. For instance, based on the obtained results, it may be expected that topology not only protects particular resonances/passbands when the resonators are being deformed, but does it also while merging or coupling of some resonances. The reflection and transmission dependences being symmetric with respect to the specific frequency, like the ones indicating possible appearance of Exceptional Points, have been found at $\phi = 0^\circ$ in the case of (nearly) the same resonators. Nevertheless, they are expected to have analogs for nonzero rotation angles, e.g., at better adjusted differences between front-side and back-side resonators, but it may need a careful optimization of the structural geometry.

At $\phi = 180^\circ$, in the case of identical resonators, we found the narrow *bridge* of nearly-perfect transmission connecting two large regions of high-transmission in the (f, S) -plane. It reminds us about the behavior of a topological mode exposed to the variations of one of the geometrical parameters. However, this analogy may be incomplete, because the obtained narrowband transmission and one of large regions of high transmission co-exist within some ranges of variations of frequency and scaling coefficient. A similar bridge was noticed in a cross-polarized transmission component at the 90-degree rotation of the back-side array. Weak and strong coupling and merging the resonances of different types and diverse scenarios of protection against simultaneous or differential deformations of the array resonators are planned to be studied at arbitrary ϕ . Besides, the collection of the results are expected to pave a path to enable new directions of research forwarded towards the realization of filters and polarization-manipulating and related AT devices with advanced multifunctional features.

Methods

The used approach is based on the intuitive predictions inspired by the earlier results, qualitative estimates and extensive numerical simulations for the justified ranges of variation of geometrical and material parameters of metastructures of the selected types. CST Studio Suite⁶⁴, an efficient commercial software based on the finite integration method, was used. This software is numerically efficient and provides controllable convergence and accuracy, that makes it particularly appropriate for the studies of metasurfaces comprising unit cells (meta-atoms) having nontrivial geometry. The frequency-domain solver with Floquet–Bloch boundary conditions and a tetrahedral mesh have been utilized to obtain the presented numerical results.

Data availability

Most of the final data generated or analysed during this study are included in this article.

Received: 21 January 2025; Accepted: 29 January 2025

Published online: 06 March 2025

References

- Smith, D. R., Padilla, W. J., Vier, D. C., Nemat-Nasser, S. C. & Schultz, S. Composite medium with simultaneously negative permeability and permittivity. *Phys. Rev. Lett.* **84**(18), 4184–4187 (2000).
- Smith, D. R. & Kroll, N. Negative refractive index in left-handed materials. *Phys. Rev. Lett.* **85**(18), 2933–2936 (2000).
- Soukoulis, C. M., Linden, S. & Wegener, M. Negative refractive index at optical wavelengths. *Science* **315**(5808), 47–49 (2007).
- Schurig, D. et al. Metamaterial electromagnetic cloak at microwave frequencies. *Science* **314**(5801), 977–980 (2006).
- Liu, N., Liu, H., Zhu, S. & Giessen, H. Stereometamaterials. *Nat. Photon.* **3**(3), 157–162 (2009).
- Shi, J. H., Ma, H. F., Guan, C. Y., Wang, Z. P. & Cui, T. J. Broadband chirality and asymmetric transmission in ultrathin 90-twisted Babinet-inverted metasurfaces. *Phys. Rev. B* **89**(16), 165128 (2014).
- Serebryannikov, A. E. et al. Ultraminiature antennas combining subwavelength resonators and a very-high- ϵ uniform substrate: The case of lithium niobate. *IEEE Trans. Antennas Propag.* **68**(7), 5071–5081 (2020).
- Dong, Y. D., Yang, T. & Itoh, T. Substrate integrated waveguide loaded by complementary split-ring resonators and its applications to miniaturized waveguide filters. *IEEE Trans. Microwave Theory Tech.* **57**(9), 2211–2223 (2009).
- Menzel, C. et al. Asymmetric transmission of linearly polarized light at optical metamaterials. *Phys. Rev. Lett.* **104**(25), 253902 (2010).
- Mutlu, M., Akosman, A. E., Serebryannikov, A. E. & Ozbay, E. Diodelike asymmetric transmission of linearly polarized waves using magnetoelectric coupling and electromagnetic wave tunneling. *Phys. Rev. Lett.* **108**(21), 213905 (2012).
- Parto, M., Liu, Y. G., Bahari, B., Khajavikhan, M. & Christodoulides, D. N. Non-Hermitian and topological photonics: Optics at an exceptional point. *Nanophotonics* **10**(1), 403–423 (2021).
- Park, S. H. et al. Observation of an exceptional point in a non-Hermitian metasurface. *Nanophotonics* **9**(5), 1031–1039 (2020).
- Liang, Y. et al. Engineering of the Fano resonance spectral response with non-Hermitian metasurfaces by navigating between exceptional point and bound states in the continuum conditions. *Opt. Express* **32**(5), 7158–7170 (2024).
- Lu, L., Ioannopoulos, J. D. & Soljačić, M. Topological photonics. *Nat. Photon.* **8**(11), 821–829 (2014).
- Nakata, Y., Ito, Y., Nakamura, Y. & Shindou, R. Topological boundary modes from translational deformations. *Phys. Rev. Lett.* **124**(7), 073901 (2020).

16. Girich, A., Ivzhenko, L., Hrinchenko, A., Tarapov, S. & Yermakov, O. Manipulation over surface waves in bilayer hyperbolic metasurfaces: Topological transition and multidirectional canalization. *IEEE Microwave Wirel. Technol. Lett.* **33**(3), 367–370 (2022).
17. Xu, H. X. et al. *Multifunctional Metasurfaces: Design Principles and Device Realizations* (Springer, Cham, 2021).
18. Aalizadeh, M., Serebryannikov, A. E., Ozbay, E. & Vandenbosch, G. A. E. A simple Mie-resonator based meta-array with diverse deflection scenarios enabling multifunctional operation at near-infrared. *Nanophoton.* **9**(15), 4589–4600 (2020).
19. Cai, T. et al. High performance bifunctional metasurfaces in transmission and reflection geometries. *Adv. Opt. Mater.* **5**, 1600506 (2017).
20. Maguid, E. et al. Multifunctional interleaved geometric-phase dielectric metasurfaces. *Light Sci. Appl.* **6**, e17027 (2017).
21. Serebryannikov, A. E., Skigin, D. C., Vandenbosch, G. A. E. & Ozbay, E. Multifunctional blazed gratings for multiband spatial filtering, retroreflection, splitting, and demultiplexing based on C2 symmetric photonic crystals. *J. Appl. Phys.* **131**(22), 223101 (2022).
22. Mandatori, A., Bertolotti, M. & Sibilìa, C. Asymmetric transmission of some two-dimensional photonic crystals. *J. Opt. Soc. Am. B* **24**(3), 685–690 (2007).
23. Serebryannikov, A. E. One-way diffraction effects in photonic crystal gratings made of isotropic materials. *Phys. Rev. B* **80**(15), 155117 (2009).
24. Stolarek, M. et al. Asymmetric transmission of terahertz radiation through a double grating. *Opt. Lett.* **38**(6), 839–841 (2013).
25. Serebryannikov, A. E. & Ozbay, E. Isolation and one-way effects in diffraction on dielectric gratings with plasmonic inserts. *Opt. Express* **17**(1), 278–292 (2009).
26. Fedotov, V. A. et al. Asymmetric propagation of electromagnetic waves through a planar chiral structure. *Phys. Rev. Lett.* **97**(16), 167401 (2006).
27. Singh, R. et al. Terahertz metamaterial with asymmetric transmission. *Phys. Rev. B* **80**(15), 153104 (2009).
28. Lv, T. et al. Dual-band dichroic asymmetric transmission of linearly polarized waves in terahertz chiral metamaterial. *Nanophotonics* **9**(10), 3235–3242 (2020).
29. Serebryannikov, A. E., Lakhtakia, A., Vandenbosch, G. A. & Ozbay, E. Transmissive terahertz metasurfaces with vanadium dioxide split-rings and grids for switchable asymmetric polarization manipulation. *Sci. Rep.* **12**, 3518 (2022).
30. Yang, W. et al. Direction-duplex Janus metasurface for full-space electromagnetic wave manipulation and holography. *ACS Appl. Mater. Interfaces* **15**(22), 27380–27390 (2023).
31. Zang, X. et al. Dual-layered metasurfaces for asymmetric focusing. *Photon. Res.* **8**(6), 830–843 (2020).
32. Chen, K. et al. Directional Janus metasurface. *Adv. Mater.* **32**(2), 1906352 (2020).
33. Mutlu, M., Cakmakyan, S., Serebryannikov, A. E. & Ozbay, E. One-way reciprocal spoof surface plasmons and relevant reversible diodelike beaming. *Phys. Rev. B* **87**(20), 205123 (2013).
34. Xu, Q. et al. Polarization-controlled asymmetric excitation of surface plasmons. *Optica* **4**(9), 1044–1051 (2017).
35. Potton, R. J. Reciprocity in optics. *Rep. Prog. Phys.* **67**(5), 717–754 (2004).
36. Liu, H. et al. Lagrange model for the chiral optical properties of stereometamaterials. *Phys. Rev. B* **81**(24), 241403 (2010).
37. Manjappa, M. et al. Tailoring the slow light behavior in terahertz metasurfaces. *Appl. Phys. Lett.* **106**(18), 181101 (2015).
38. Fan, S., Suh, W. & Joannopoulos, J. D. Temporal coupled-mode theory for the Fano resonance in optical resonators. *J. Opt. Soc. Am. A* **20**(3), 569–572 (2003).
39. Hao, X. et al. Twisted stacking metasurface for complete amplitude and phase control of circularly polarized terahertz waves. *Laser Photon. Rev.* **18**(12), 2400644 (2024).
40. Khan, M. I., Fraz, Q. & Tahir, F. A. Ultra-wideband cross polarization conversion metasurface insensitive to incidence angle. *J. Appl. Phys.* **121**(4), 045103 (2017).
41. Kamal, B. et al. High efficiency and ultra-wideband polarization converter based on an L-shaped metasurface. *Opt. Mater. Express* **11**(5), 1343–1352 (2021).
42. Inokuma, A. et al. Broadband and efficient terahertz helicity inversion by a reconfigurable reflective metasurface based on vanadium dioxide. *Appl. Phys. Lett.* **125**(8), 081703 (2024).
43. Grady, N. K. et al. Terahertz metamaterials for linear polarization conversion and anomalous refraction. *Science* **340**(6138), 1304–1307 (2013).
44. Cuartero-González, A., Sanders, S., Zundel, L., Fernández-Domínguez, A. I. & Manjavacas, A. Super- and subradiant lattice resonances in bipartite nanoparticle arrays. *ACS Nano* **14**(9), 11876–11887 (2020).
45. Kravets, V. G., Kabashin, A. V., Barnes, W. L. & Grigorenko, A. N. Plasmonic surface lattice resonances: A review of properties and applications. *Chem. Rev.* **118**(12), 5912–5951 (2018).
46. Castellanos, G. W., Bai, P. & Gómez Rivas, J. Lattice resonances in dielectric metasurfaces. *J. Appl. Phys.* **125**(21), 213105 (2019).
47. Humphrey, A. D. & Barnes, W. L. Plasmonic surface lattice resonances on arrays of different lattice symmetry. *Phys. Rev. B* **90**(7), 075404 (2014).
48. Liu, T., Xu, R., Yu, P., Wang, Z. & Takahara, J. Multipole and multimode engineering in Mie resonance-based metastructures. *Nanophotonics* **9**(5), 1115–1137 (2020).
49. Vakevainen, A. I. et al. Plasmonic surface lattice resonances at the strong coupling regime. *Nano Lett.* **14**(4), 1721–1727 (2014).
50. Shung, K. W. K. & Tsai, Y. C. Surface effects and band measurements in photonic crystals. *Phys. Rev. B* **48**(15), 11265–11269 (1993).
51. Serebryannikov, A. E., Lakhtakia, A. & Ozbay, E. Single and cascaded, magnetically controllable metasurfaces as terahertz filters. *J. Opt. Soc. Am. B* **33**(5), 834–841 (2016).
52. Miroshnichenko, A. E., Flach, S. & Kivshar, Y. S. Fano resonances in nanoscale structures. *Rev. Mod. Phys.* **82**(3), 2257–2298 (2010).
53. Reynolds, A. L. et al. Coupled defects in photonic crystals. *IEEE Trans. Microwave Theory Techn.* **49**(10), 1860–1867 (2001).
54. Bayindir, M., Temelkuran, B. & Ozbay, E. Tight-binding description of the coupled defect modes in three-dimensional photonic crystals. *Phys. Rev. Lett.* **84**(10), 2140–2143 (2000).
55. Costa, A. E. B., Mejía-Salazar, J. R. & Cavalcanti, S. B. Defect modes in metamaterial photonic superlattices as tunneling resonances in trilayer structures. *J. Opt. Soc. Am. B* **33**(3), 468–473 (2016).
56. Lepetit, T., Akmansoy, E., Ganne, J. P. & Lourtioz, J. M. Resonance continuum coupling in high-permittivity dielectric metamaterials. *Phys. Rev. B* **82**(19), 195307 (2010).
57. Lepetit, T. & Kanté, B. Controlling multipolar radiation with symmetries for electromagnetic bound states in the continuum. *Phys. Rev. B* **90**(24), 241103 (2014).
58. Huang, L. et al. Ultrahigh-Q guided mode resonances in an all-dielectric metasurface. *Nat. Commun.* **14**, 3433 (2023).
59. Kim, S. J. & Brongersma, M. L. Active flat optics using a guided mode resonance. *Opt. Lett.* **42**(1), 5–8 (2016).
60. Cao, G. et al. Fano resonance in artificial photonic molecules. *Adv. Opt. Mater.* **8**(10), 1902153 (2020).
61. Calvo, M. R., Jacob, D. & Untiedt, C. Analysis of the Kondo effect in ferromagnetic atomic-sized contacts. *Phys. Rev. B* **86**(7), 075447 (2012).
62. Hu, C. et al. A metasurface with bidirectional hyperbolic surface modes and position-sensing applications. *NPG Asia Mater.* **10**(5), 417–428 (2018).
63. Gokkavas, M., Gundogdu, T. F., Ozbay, E. & Serebryannikov, A. E. Few-layer bifunctional metasurfaces enabling asymmetric and symmetric polarization-plane rotation at the subwavelength scale. *Sci. Rep.* **14**, 13636 (2024).
64. See <https://www.3ds.com/products-services/simulia/products/cst-studio-suite/solvers/>.

Acknowledgements

This work was supported by NAWA, PHC POLONIUM grant, project DYNAMET, contract number BPN/BFR/2022/1/00023/U/00001. We also thank Grand Valley State University's Open Access Publishing Support as well as CSCE funds.

Author contributions

A. E. S. and A. O. C. suggested the concept. A. E. S., A. O. C. and E. C. performed numerical simulations. A. E. S. and E. C. contributed to the results analysis. All authors contributed to the formulation of the goals of the study, and writing and reviewing the manuscript.

Declarations

Competing interests

The authors declare no competing interests.

Additional information

Correspondence and requests for materials should be addressed to A.O.C.

Reprints and permissions information is available at www.nature.com/reprints.

Publisher's note Springer Nature remains neutral with regard to jurisdictional claims in published maps and institutional affiliations.

Open Access This article is licensed under a Creative Commons Attribution-NonCommercial-NoDerivatives 4.0 International License, which permits any non-commercial use, sharing, distribution and reproduction in any medium or format, as long as you give appropriate credit to the original author(s) and the source, provide a link to the Creative Commons licence, and indicate if you modified the licensed material. You do not have permission under this licence to share adapted material derived from this article or parts of it. The images or other third party material in this article are included in the article's Creative Commons licence, unless indicated otherwise in a credit line to the material. If material is not included in the article's Creative Commons licence and your intended use is not permitted by statutory regulation or exceeds the permitted use, you will need to obtain permission directly from the copyright holder. To view a copy of this licence, visit <http://creativecommons.org/licenses/by-nc-nd/4.0/>.

© The Author(s) 2025, corrected publication 2025